lacking senGC activation mediators may be related to loss of senGC protection (*4*, *5*, *27*). DSS triggered inflammasome activity localized to upper-crypt cells and led to depletion of senGCs (Fig. 6, C to F). Ex vivo experiments confirmed that senGC-mediated mucus secretion displaced bacteria from crypt openings (Fig. 6, A and B), and senGC activation after inner mucus layer disruption likely generates a similar response. Depletion of senGCs by repeated challenge would leave the crypt without defense—an event that may be important in understanding the development of chronic colitis.

## REFERENCES AND NOTES


1. M. E. V. Johansson *et al.*, *Proc. Natl. Acad. Sci. U.S.A.* **105**, 15064–15069 (2008).
2. D. Ambort *et al.*, *Proc. Natl. Acad. Sci. U.S.A.* **109**, 5645–5650 (2012).
3. A. Velcich *et al.*, *Science* **295**, 1726–1729 (2002).
4. S. Rakoff-Nahoum, J. Paglino, F. Eslami-Varzaneh, S. Edberg, R. Medzhitov, *Cell* **118**, 229–241 (2004).
5. A. L. Frantz *et al.*, *Mucosal Immunol.* **5**, 501–512 (2012).
6. M. Lamkanfi, V. M. Dixit, *Cell* **157**, 1013–1022 (2014).
7. E. Elinav *et al.*, *Cell* **145**, 745–757 (2011).
8. M. E. V. Johansson, *PLOS ONE* **7**, e41009 (2012).
9. K. A. Knoop, K. G. McDonald, S. McCrate, J. R. McDole, R. D. Newberry, *Mucosal Immunol.* **8**, 198–210 (2015).
10. M. Wlodarska *et al.*, *Cell* **156**, 1045–1059 (2014).
11. D. R. Halm, S. T. Halm, *Am. J. Physiol.* **277**, C501–C522 (1999).
12. J. K. Gustafsson *et al.*, *Am. J. Physiol.* **302**, G430–G438 (2012).
13. See supplementary materials on *Science* Online.
14. R. Zhou, A. Tardivel, B. Thorens, I. Choi, J. Tschopp, *Nat. Immunol.* **11**, 136–140 (2010).
15. F. Bauernfeind *et al.*, *J. Immunol.* **187**, 613–617 (2011).
16. R. D. Specian, M. R. Neutra, *J. Cell Biol.* **85**, 626–640 (1980).
17. M. E. V. Johansson *et al.*, *PLOS ONE* **5**, e12238 (2010).
18. H. E. Jakobsson *et al.*, *EMBO Rep.* **16**, 164–177 (2015).
19. M. E. V. Johansson *et al.*, *Gut* **63**, 281–291 (2014).
20. K. S. B. Bergstrom *et al.*, *PLOS Pathog.* **6**, e1000902 (2010).
21. J. R. McDole *et al.*, *Nature* **483**, 345–349 (2012).
22. P. C. Colony, R. D. Specian, *Anat. Rec.* **218**, 365–372 (1987).
23. A. Panday, M. K. Sahoo, D. Osorio, S. Batra, *Cell. Mol. Immunol.* **12**, 5–23 (2015).
24. K. K. Patel *et al.*, *EMBO J.* **32**, 3130–3144 (2013).
25. M. E. Sellin *et al.*, *Cell Host Microbe* **16**, 237–248 (2014).
26. L. A. Knodler *et al.*, *Cell Host Microbe* **16**, 249–256 (2014).
27. D. Demon *et al.*, *Mucosal Immunol.* **7**, 1480–1491 (2014).


## ACKNOWLEDGMENTS


Supported by the Swedish Research Council, Swedish Cancer Foundation, Knut and Alice Wallenberg Foundation, Lundberg Foundation, Sahlgren's University Hospital (ALF), Torsten Söderbergs Stiftelse, National Institute of Allergy and Infectious Diseases grant U01AI095473, and Swedish Foundation for Strategic Research. We thank the Gothenburg Centre for Cellular Imaging for technical help, F. Svensson for generating the RedMUC2$^{98trTg}$ mice, and W.-D. Hardt and the Mucosal Immunobiology and Vaccine Center at the University of Gothenburg for mouse strains.


## SUPPLEMENTARY MATERIALS

www.sciencemag.org/content/352/6293/1535/suppl/DC1
Materials and Methods
Figs. S1 to S7
Movies S1 to S7
Reference (*28*)


23 March 2016; accepted 16 May 2016
10.1126/science.aaf7419


STRUCTURAL BIOLOGY

# Atomic structure of Hsp90-Cdc37-Cdk4 reveals that Hsp90 traps and stabilizes an unfolded kinase


**Kliment A. Verba,[1] Ray Yu-Ruei Wang,[1] Akihiko Arakawa,[2] Yanxin Liu,[1] Mikako Shirouzu,[2] Shigeyuki Yokoyama,[2] David A. Agard[1]***



**The Hsp90 molecular chaperone and its Cdc37 cochaperone help stabilize and activate more than half of the human kinome. However, both the mechanism by which these chaperones assist their "client" kinases and the reason why some kinases are addicted to Hsp90 while closely related family members are independent are unknown. Our structural understanding of these interactions is lacking, as no full-length structures of human Hsp90, Cdc37, or either of these proteins with a kinase have been elucidated. Here we report a 3.9 angstrom cryo–electron microscopy structure of the Hsp90-Cdc37-Cdk4 kinase complex. Surprisingly, the two lobes of Cdk4 are completely separated with the β4-β5 sheet unfolded. Cdc37 mimics part of the kinase N lobe, stabilizing an open kinase conformation by wedging itself between the two lobes. Finally, Hsp90 clamps around the unfolded kinase β5 strand and interacts with exposed N- and C-lobe interfaces, protecting the kinase in a trapped unfolded state. On the basis of this structure and an extensive amount of previously collected data, we propose unifying conceptual and mechanistic models of chaperone-kinase interactions.**


The human kinome is responsible for regulating about one-third of all proteins through phosphorylation (*1*). Proper regulation of this process is important, as misregulated kinase activity can lead to cell death and disease (*2*). To achieve fine regulation, kinase activity can be sensitively modulated by multiple allosteric inputs. Thus, kinase domains are organized so that dispersed small structural changes caused by binding of regulatory domains and proteins or phosphorylation can substantially alter kinase activity. Examples of such regulatory interactions abound, with SH2 and SH3 domains for Src family kinases, dimerization for epidermal growth factor receptor (EGFR) or Raf family kinases, and cyclin regulation for Cdks being well-characterized examples (*3*).

Beyond these specific regulators, the Hsp90 molecular chaperone, a member of the general cellular protein-folding machinery, also plays a fundamental role in the regulation of many kinases (*4*). Though chaperones usually facilitate the early steps of protein folding, Hsp90 also functions late in the process to help both fold and activate a set of protein "clients" (~10% of the proteome) (*5*). Notably, ~60% of the human kinome interacts with Hsp90, with the assistance of its kinase-specific cochaperone, Cdc37 (*6*). Pharmocologic inhibition of Hsp90 leads to rapid ubiquitinylation and degradation of client kinases. Because many Hsp90- and Cdc37-dependent kinases are key oncoproteins, (vSrc, bRafV600E, Her2, etc.), several Hsp90 inhibitors are undergoing clinical trials as cancer therapeutics (*7*).

Hsp90 is a well-conserved but highly dynamic molecular machine. Each monomer within the Hsp90 dimer has three structural domains: a C-terminal domain (CTD) responsible for dimerization, a middle domain (MD) implicated in client binding, and an N-terminal domain (NTD) that binds adenosine triphosphate (ATP). Without bound nucleotide, Hsp90 mostly populates a variety of open states, whereas nucleotide binding promotes the formation of a closed state in which the NTDs also dimerize, followed by hydrolysis (*8*, *9*). The rates of closure and hydrolysis are homolog-specific, with human cytosolic Hsp90s almost always open, whereas yeast Hsp90 preferentially adopts a fully closed state (*10*). Toward the end of the NTD is a highly charged region (i.e., a charged linker) that shows wide variation in length and composition between species. The function and structure of this charged linker are unclear, but deletion can affect Hsp90 function (*11*).

Cdc37 is less well studied. The monomeric protein can also be divided into three domains: an NTD of unknown structure that interacts with kinases, a globular MD that interacts with Hsp90, and an extended CTD of unknown function (*12*). Although there is a cocrystal structure of the Cdc37 MD and CTD (Cdc37 M/C) bound to the Hsp90 NTD (*13*), there is evidence that Cdc37 may also interact with the MD of Hsp90 (*14*). Phosphorylation of Cdc37 Ser$^{13}$ plays an important role, providing stabilizing interactions in vitro (*15*) and being functionally necessary in vivo (*16*).

Although a wealth of in vivo data has been collected, a physical understanding of how Hsp90


[1]Howard Hughes Medical Institute (HHMI) and the Department of Biochemistry and Biophysics, University of California San Francisco, San Francisco, CA 94158, USA. [2]RIKEN Systems and Structural Biology Center, 1-7-22 Suehiro-cho, Tsurumi-ku, Yokohama 230-0045, Japan.
***Corresponding author. Email: agard@msg.ucsf.edu**

and Cdc37 facilitate kinase function is lacking. Equally unclear is why some kinases are strongly dependent on Hsp90, whereas closely related kinases function independently. Despite numerous attempts to identify a consistent motif responsible for Hsp90 interaction, the only general trend that has emerged is that client kinases appear to be less thermally stable than nonclients (*6*). Supporting this notion, the binding of kinase inhibitors or allosteric regulators reduces Hsp90 interactions (*17*, *18*). Though it is reasonable that less-stable kinases might depend on Hsp90, it remains unclear why this happens or what Hsp90 recognizes. Despite its obvious value, the crystal structure of an Hsp90-Cdc37-kinase complex has remained elusive, probably due to the dynamic nature of Hsp90-client interactions and challenges in reconstituting the complex. Encouraged by previous negative-stain electron microscopy (EM) studies (*19*) and the recent advances in cryo-EM detectors and processing methodologies that together make it feasible to analyze such a small, asymmetric complex (*20*), we undertook cryo-EM studies of the human 240-kDa Hsp90-Cdc37-Cdk4 kinase complex.

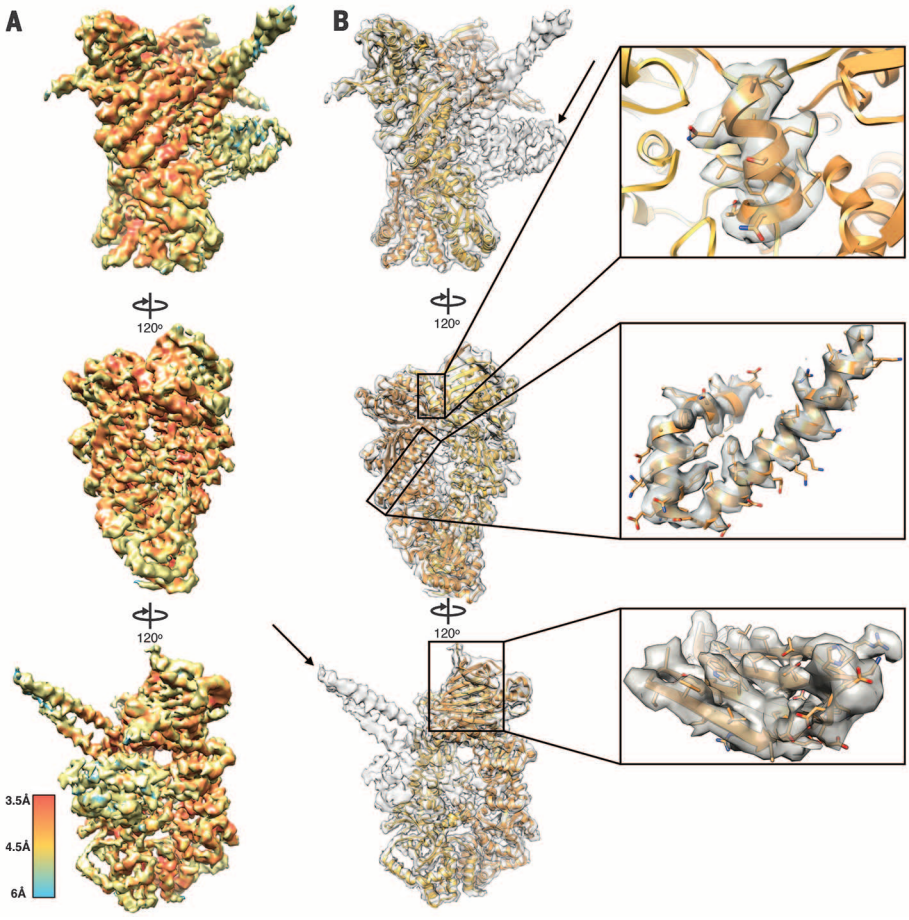


**Fig. 1. The 4 Å map of Hsp90-Cdc37-Cdk4.** (**A**) Density map colored by resolution. (**B**) hHsp90β model built into the density map, with different monomers depicted in shades of orange. Insets show high-resolution features. Arrows indicate density unaccounted for by Hsp90.

## Complex formation and cryo-EM structural analysis

Human homologs of all three proteins were co-expressed in Sf9 insect cells. A stable ternary complex that survived rigorous dual-tag purification formed in the presence of molybdate (fig. S1). Although the mode of molybdate action is unknown, it affects Hsp90's hydrolysis rate and helps stabilize Hsp90-client interactions (*21*). Simply mixing components individually purified from insect cells did not yield any detectable complex; therefore, either posttranslational modifications specific to the complex or other components (like Hsp40 or Hsp70) are required. Despite considerable effort to optimize conditions and image processing, preferential particle orientation and conformational heterogeneity limited initial reconstructions from data collected in house to about 6 to 8 Å resolution. To move forward, a much larger data set was collected at the National Resource for Automated Molecular Microscopy (NRAMM) (*22*). Data quality was

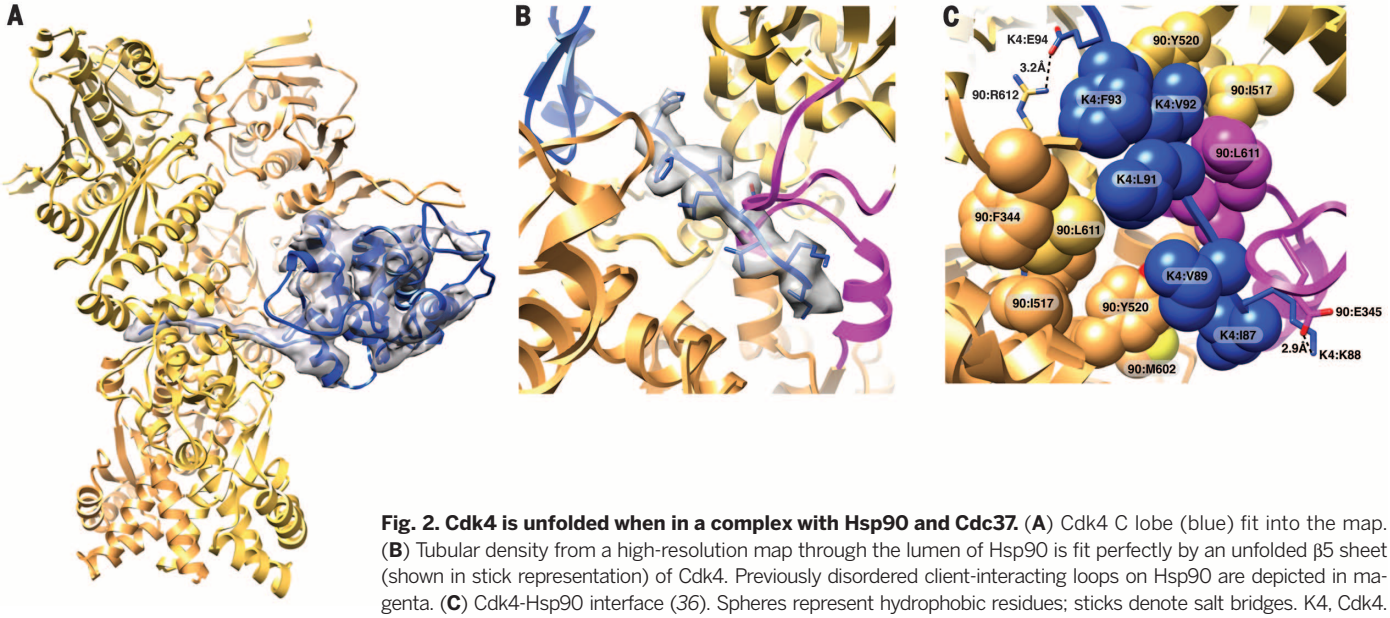


**Fig. 2. Cdk4 is unfolded when in a complex with Hsp90 and Cdc37.** (**A**) Cdk4 C lobe (blue) fit into the map. (**B**) Tubular density from a high-resolution map through the lumen of Hsp90 is fit perfectly by an unfolded β5 sheet (shown in stick representation) of Cdk4. Previously disordered client-interacting loops on Hsp90 are depicted in magenta. (**C**) Cdk4-Hsp90 interface (*36*). Spheres represent hydrophobic residues; sticks denote salt bridges. K4, Cdk4.

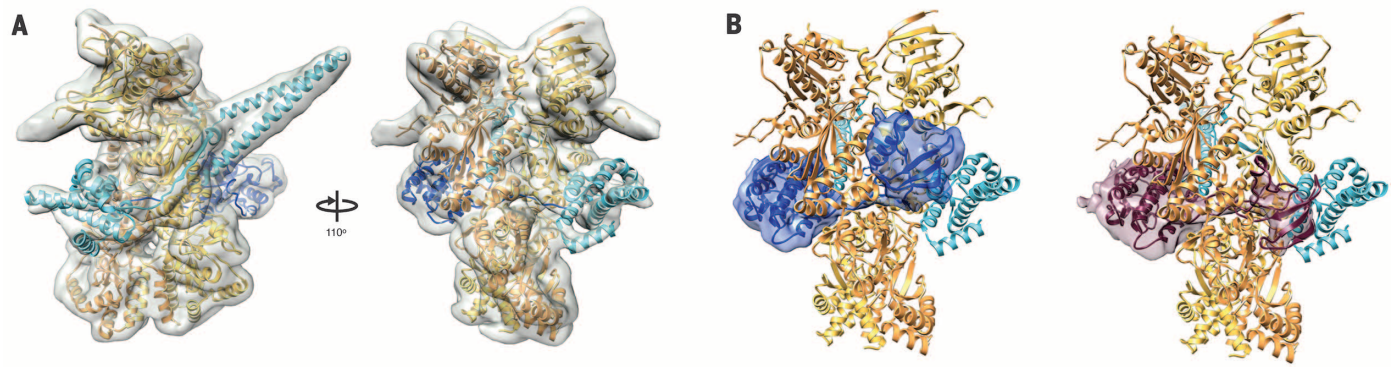


**Fig. 3. Rounds of focused 3D classification yield distinct densities for Cdc37 and the Cdk4 N lobe.** (**A**) One of the new classes has clear density for the Cdc37 M/C fragment crystal structure. Our complete Cdc37 model (residues 1 to 260) is shown in teal. Note the β strand wrapping around the outside of Hsp90, connecting the two major Cdc37 domains. (**B**) Two additional classes show previously unobserved density for the missing Cdk4 N lobe. These classes, minus the Hsp90-Cdc37 density highlight the two previously unseen Cdk4 N-lobe conformations (shown in blue and maroon, respectively). Fitted kinase models are illustrated as ribbons.

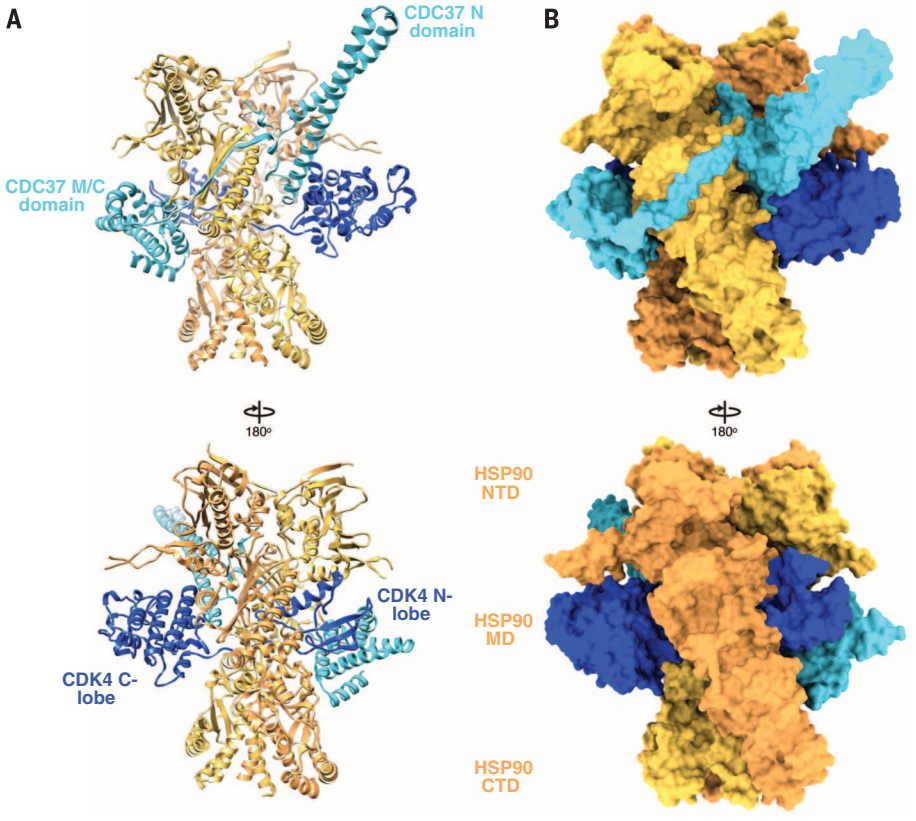


**Fig. 4. Hsp90, Cdc37, and Cdk4 are intricately interwoven in the complex.** Two views of the complete model, depicted in ribbon representation in (**A**) and surface representation in (**B**).

verified, as two-dimensional (2D) classification of ~800,000 initially chosen particles yielded classes with visible high-resolution features (fig. S2). Three-dimensional classification and refinement resulted in a 4 Å map (figs. S3 and S4 and table S1), with most of the Hsp90 structure being better resolved (3.5 Å), whereas the lowest-resolution regions were ~6 Å (Fig. 1A).

## Hsp90 is in a closed conformation in the complex

Refining the 4 Å map with a tighter mask around Hsp90 resulted in a higher-resolution, 3.9 Å density for Hsp90 and neighboring regions (Fig. 1B, insets) (*22*). This map was of sufficient quality to accurately build and refine an atomic model of human Hsp90β based on a homology model derived from yeast Hsp90 (Fig. 1B and fig. S5). Surprisingly, reconstructions of the complex prepared with Hsp90 with a deleted charged linker never yielded good results, probably due to increased heterogeneity. Hsp90 adopts a symmetrical [root mean square deviation (RMSD) between monomers = 0.82 Å] closed conformation, which closely resembles the yHsp90 closed state (*23*). This result was unexpected, as without a cross-linker, closed hHsp90 had not been previously observed. Although the molybdate added during purification may contribute, the closed state is probably a consequence of the ternary complex. In our map, which was refined without symmetry, the strongest density is symmetric at the γ-phosphate location for nucleotide binding sites at both NTDs of Hsp90 (fig. S6). This suggests that either the complex traps Hsp90 in an ATP state or, more likely, ADP·molybdate acts as a posthydrolysis transition state inhibitor, thereby helping to stabilize the closed conformation. The hHsp90 model determined here is similar to the yeast Hsp90 structure (RMSD = 1.59 Å), with a small rotation in the CTD and correlated movements throughout (movie S1). Additionally, a number of loops disordered in the crystal structure were ordered in our model, as they were interacting with the kinase (Fig. 2B). The charged linker is visible in 2D classes but is absent from the 3D reconstruction, suggesting a highly flexible structure (fig. S2).

## The N lobe of Cdk4 is substantially unfolded and threads through Hsp90

Two regions of the 4 Å map cannot be accounted for by Hsp90: a long coiled-coil like protrusion and a globular density on one side of Hsp90 (arrows in Fig. 1B). Although we initially suspected that these regions correspond to the Cdc37 M/C (globular domain with long helix), the globular domain fit became worse as our map improved. To obtain an unbiased fit, we performed an exhaustive search against all protein folds in the CATH database [~16,000 Protein Data Bank identifiers (PDB IDs)] (*22*). Disregarding algorithmic

errors, the top-scoring hits were all variations on the kinase C lobe, with Cdc37 M/C scoring considerably worse (fig. S7). Based on these findings, the Cdk4 C lobe was placed into the density (*24*), resulting in a high-quality fit (Fig. 2A). By contrast, not only does no suitable density exist for the folded kinase N lobe, but it would also sterically clash with Hsp90. Notably, however, tracing the kinase density from the C lobe toward the N terminus, there was a clear tubular region going through the lumen of Hsp90 (Fig. 2, A and B). Thus, a drastically altered conformation of the kinase N lobe is being stabilized by Hsp90 (movie S2). Threading the Cdk4 sequence into this density reveals that the β4 and β5 strands have been ripped apart, and instead β5 interacts with a previously mapped general Hsp90 client binding site via extensive hydrophobic interactions (*25*) and two salt bridges (Fig. 2C). Potentially due to these interactions, the Hsp90 CTD rotates toward the kinase (as compared to the yHsp90 structure) at the MD-CTD interface, which was identified as asymmetric in previous work (*26*) (movie S1). Altogether, this suggests that the MD-CTD interface may be used to communicate Hsp90's hydrolysis state to the client. Unfortunately, in the highest-resolution map, no density was visible for kinase residues at the N-terminal end of the β5 strand.

## Cdc37 is split into two domains and wraps around Hsp90

Although there is no available 3D structural information for the Cdc37 NTD, sequence analysis (MARCOIL) predicts a significant coiled-coil structure. Supported by our observations of high helical content, as determined by circular dichroism and nuclear magnetic resonance (fig. S8), a coiled-coil provides a good candidate for the nonglobular map density (Fig. 1B). That density transitions from helical to strandlike, wrapping around the Hsp90 MD and adding an additional β strand to the 1AC β sheet (PDB ID 2CG9). Unfortunately, as with the kinase, this β strand does not connect to any density on the other side, thwarting a complete fit of Cdc37. Demonstrating the power of single-particle cryo-EM, local rounds of 3D classification yielded a 7 Å map (figs. S3 and S9) showing clear globular density that is connected through the β strand to the coiled-coil region (Fig. 3A). This previously unobserved density was unambiguously fit by the crystallized Cdc37 M/C fragment. Using a combination of the two maps, we were able to fit Cdc37 M/C residues 148 to 260 and de novo build residues 1 to 147 of human Cdc37 (Fig. 3A) (*22*). Although further classification revealed some density beyond residue 260, it was too weak to model with confidence.

## Locating the remainder of the kinase N lobe and verification

The local 3D classification also revealed the remainder of the kinase N lobe (Fig. 3B and movie S3). In two of the classes, distinct globular densities were visible that connected to the tubular density derived from the unfolded Cdk4 N lobe. At the same time, the density for the MD of Cdc37 was either very weak or absent, suggesting an anticorrelation between Cdc37 M/C–Hsp90 interactions and kinase N-lobe–Hsp90 interactions. We were able to roughly fit the rest of the Cdk4 N lobe into these densities, allowing us to build a complete model of the Hsp90-Cdc37-Cdk4 complex (Fig. 4 and movie S4). Given the unusual split domain conformation for both the kinase and the cochaperone, it was important to verify our structural assignments. Toward that end, we used T4 lysozyme to covalently tag Cdc37 at its N terminus and Cdk4 at its C terminus. The two different complexes were expressed and purified from yeast, followed by cryo-EM reconstruction of each. These two structures clearly show lysozyme

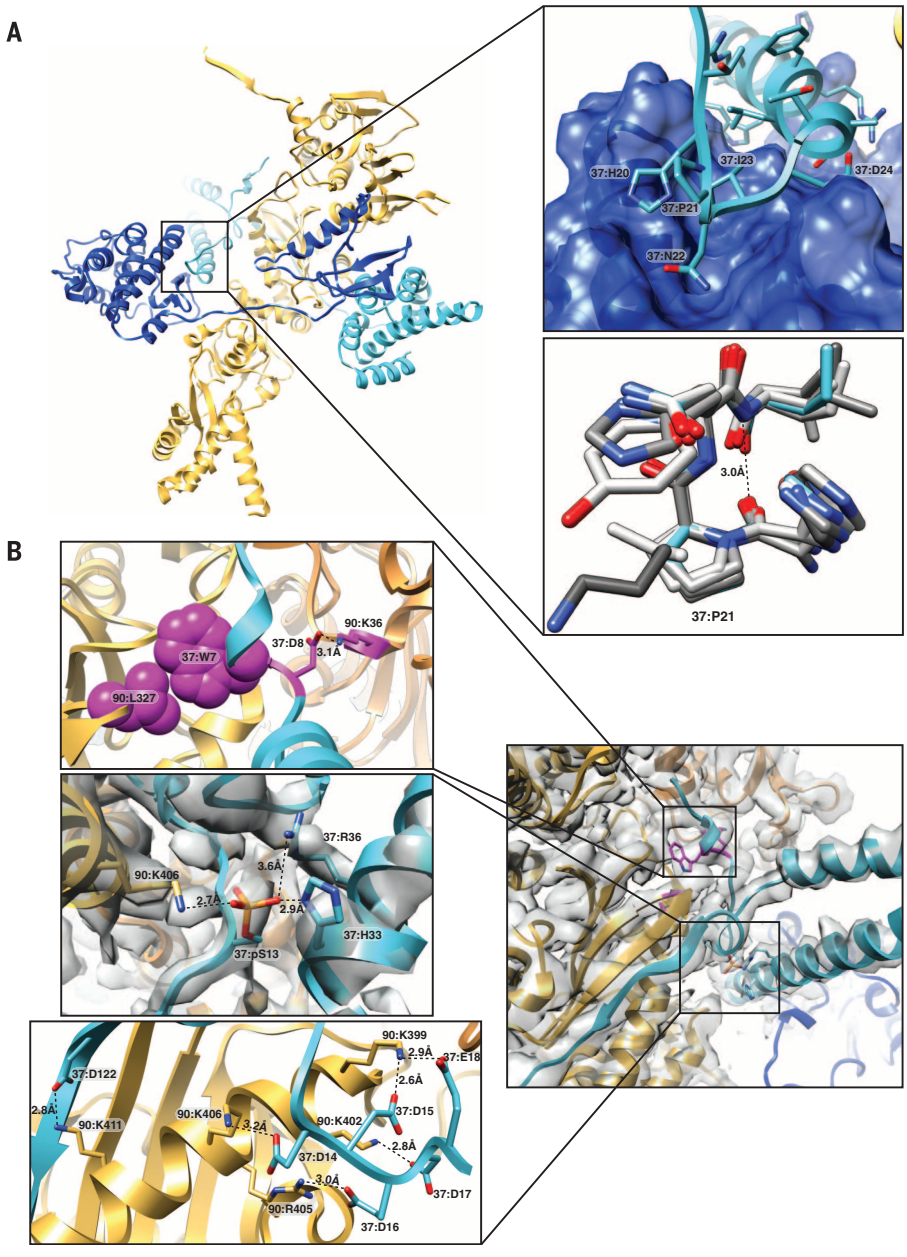


**Fig. 5. High-resolution details of Cdc37 interactions with Hsp90 and Cdk4.** (**A**) Overall arrangement of Hsp90-Cdc37-Cdk4 (one Hsp90 monomer removed for clarity). The insets highlight Cdc37-Cdk4 interaction features: (Top) Cdc37 and Cdk4 interact via hydrophobic interactions and backbone hydrogen bonds, with perfect shape complementarity. (Bottom) Overlay of Cdc37's conserved HPN motif (teal) perfectly mimicking a type I β turn of the αC-β4 loop of six different kinases (shades of gray) (PDB IDs: 3G33, 2ITP, 1QMZ, 3PP0, 1JNK, and 4FK3). (**B**) Zooming in on Hsp90-Cdc37 interactions. (Top inset) Cdc37-Hsp90 interactions mimic previously identified p23-Hsp90 interactions (magenta). (Middle inset) Phospho-Ser[13] stabilizes the local Cdc37 structure through interactions with conserved R36 and H33 and also interacts with Hsp90 at K406. (Bottom inset) Six salt bridges stabilize Hsp90-Cdc37 interactions.

density consistent with our map interpretation (fig. S10).

### Cdc37 precisely mimics a conserved feature of kinase N-lobe–C-lobe interactions and makes previously unseen interactions with Hsp90

The resulting model (Fig. 4) contains a number of notable features that explain a wealth of accumulated, seemingly contradictory observations. The Cdc37 NTD forms a long coiled-coil with a leucine zipper-like motif. The N terminus of this coiled-coil interacts with Cdk4 through extensive hydrophobic and hydrogen bonding interactions, burying 725 Å$^2$ (table S2) in surface area, and mimicking interactions that the kinase αC-β4 loop normally makes with the C lobe (Fig. 5A). Additionally, the following loop in Cdc37 overlays perfectly with the αC-β4 loop of multiple kinases, packing tightly against the kinase C lobe (Fig. 5A, bottom inset), revealing why this Cdc37 region is so conserved (fig. S11). Thus, Cdc37 binds to the kinase C lobe by mimicking interactions the N lobe normally makes, stabilizing separation of the two kinase lobes.

The interactions between Cdc37 and Hsp90 are considerably different from those seen in the previous crystal structure of fragments of each protein. Instead of binding to an Hsp90 NTD surface that would be accessible only in the open state, Cdc37 M/C interacts with the Hsp90 MD in the Hsp90 closed state, although these interactions are fairly limited (only ~340 Å$^2$ out of 2650 Å$^2$ total buried surface area) (Fig. 4). Interactions with Cdc37 residues 120 to 129, which pack a β strand against Hsp90 MD (Fig. 5B), are more extensive. Additionally, part of the Cdc37 NTD binds to a new site on the closed Hsp90 NTD, somewhat mimicking interactions seen between p23 and Hsp90 (Fig. 5B, top inset). There is also an extensive network of ionic interactions between Cdc37 NTD and Hsp90 MD, which explains previously identified salt sensitivity of Cdc37-Hsp90 binding (Fig. 5B, bottom inset). Our structure thus helps to explain recent data indicating that *Caenorhabditis elegans* Cdc37 interacts with the MD of Hsp90 (*27*), rather than the NTD, as observed in previous human domain binding studies. Instead of assuming that *C. elegans* is different or that the interactions observed with isolated domains were incorrect, we propose that Cdc37-kinase first binds Hsp90 in its open conformation, as seen in the crystal structure, and then rearranges to the site on the MD upon Hsp90 closure, as seen in our structure.

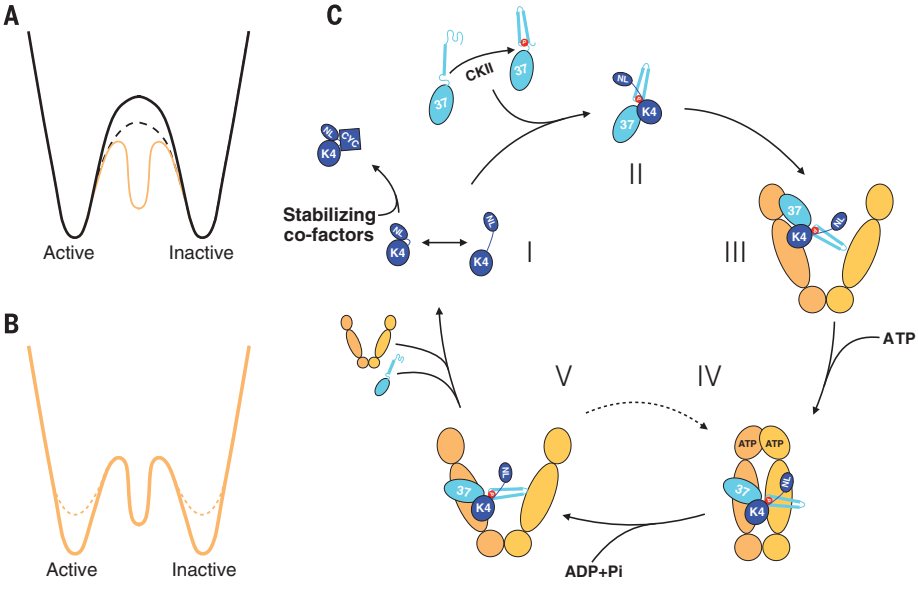


**Fig. 6. Conceptual model for linkage between kinase folding and activation and proposed model for the Hsp90-Cdc37-kinase cycle.** (**A**) Transitioning between states through an unfolded intermediate (black dashed line) has a lower energy barrier compared with that for transitioning through rigid-body motion (black solid line). The Hsp90-Cdc37 complex stabilizes such an unfolded intermediate (orange solid line). (**B**) By comparison with nonclients (orange solid line), the active and inactive states of client kinases (orange dashed lines) are destabilized. (**C**) Speculative model for an Hsp90-Cdc37-kinase cycle. (I) The kinase domain transiently samples an open state. Interactions with cofactors (such as cyclins, SH2 and SH3 domains, etc.) stabilize the kinase native state, disfavoring the open state (NL, N lobe; CYC, cyclin; K4, Cdk4). Casein kinase 2 (CKII)–phosphorylated Cdc37 (37) captures the open state by binding the kinase C lobe (II). Cdc37-kinase then binds to open Hsp90 (III). Hsp90 binds to ATP and closes upon the unfolded part of the kinase. Cdc37 migrates down, resulting in the structure described here (IV). Upon hydrolysis of ATP, Hsp90 opens with Cdc37-Cdk4 still bound, providing a chance for the kinase to fold (V). If it folds, it displaces Cdc37 and leaves the complex. If, however, it fails to displace Cdc37, then Hsp90 is able to rebind ATP and go back to state IV, repeating the process. At some point during this cycle, PP5 phosphatase is recruited to the complex to dephosphorylate Cdc37. Pi, phosphate.

### Phosphorylation of Cdc37 stabilizes the kinase-bound conformation

Phosphorylation at the completely conserved Ser$^{13}$ residue of Cdc37 is important for kinase function and was thought to be directly involved in kinase binding (*15*, *16*). In our structure, there is density for the phosphorylated Ser$^{13}$, which forms a salt bridge with Cdc37-Arg$^{36}$ and Cdc37-His$^{33}$, stabilizing the N terminus of the coiled coil (Fig. 5B, middle inset). This provides a molecular rationale for previous observations of a Cdc37 conformational change upon phosphorylation (*28*). Of note, this phosphate also contributes to the overall electrostatic nature of Hsp90-Cdc37 interactions, by forming a salt bridge with Hsp90-Lys$^{406}$. The residues making up the Cdc37–Hsp90 NTD and Cdc37-kinase interaction surfaces are extremely well conserved (fig. S11), further validating the importance of the interactions observed here.

### Hsp90 and Cdc37 capture and stabilize structural transitions within the kinase

In the ternary complex, Cdk4 assumes a conformation substantially different from those previously observed for any kinase structure. The kinase hinge region and the β4-β5 sheet are completely unfolded, with the N and C lobes being pried apart and stabilized by the interactions with Hsp90 and Cdc37. On the basis of this conformation, we propose a model where it is the propensity for the kinase to unfold to an N-lobe–C-lobe separated open state rather than a specific binding sequence that determines whether a particular kinase will be a client. Furthermore, the fact that many nonclient kinases depend on Hsp90 during initial folding would suggest that the open kinase state we observe is an on-pathway folding intermediate.

In agreement with the model, the β3-αC loop of Cdk4 (strong client) has seven glycine residues versus one or two glycines in the same loop of Cdk2 and Cdk6 (nonclient and weak client, respectively). Mutating this loop in Cdk4 to the Cdk6 sequence stabilizes the protein (*29*). In a similar manner, a single point mutation derived from EGFR (nonclient) in the αC-β4 loop was able to abrogate the interactions of HER2 (strong client) with, and its dependence on, Hsp90-Cdc37 (*30*). This point mutation would potentially introduce a salt bridge to stabilize the kinase loop (fig. S12) and, hence, the association between the kinase lobes.

Our model explains why a sequence motif responsible for Hsp90 interactions has yet to be found. The allosteric properties of kinases allow distant and seemingly unrelated mutations to destabilize the N-lobe–C-lobe interface, explaining often-confusing mutagenesis results. Thus, nonclient kinases would exit Hsp90 dependence after initial folding via stabilizing interactions with regulatory partners or extra domains (cyclin, dimerization partners, SH2 and SH3 domains, etc.).

### Linking kinase unfolding to assembly and activity

Why might it be beneficial for a large percentage of human kinases to substantially populate a

folding intermediate, even when mature? Rather than being a vestige of kinase evolution with Hsp90 buffering gain-of-function destabilizing mutations (*31*), we argue that being able to safely populate such an open folding intermediate has a direct functional and regulatory benefit. Recent computational efforts have suggested a connection between folding and kinase activity (*32*, *33*). The concept is that the most favorable transition between the inactive and active states is through a more open, unfolded state rather than through a more classical rigid-body transition. Although the opening seen in simulations is far more subtle than what we observed, we suggest that the concept still applies (Fig. 6A). The generally lower stability of client kinases would lead to enhanced sampling of the open state, thereby encouraging chaperone binding (Fig. 6B). Chaperone stabilization of a kinase open state could increase the overall rates of interconversion and/or protect a potentially vulnerable state from aggregation or recognition by the ubiquitinylation machinery. Moreover, the open state could be the preferred substrate for adding and removing posttranslational modifications, as well as for critical stabilizing interactions.

### Life cycle of kinase-Hsp90-Cdc37 interactions

Our structure also suggests how the observed state might arise and mature (Fig. 6C). Hsp90 would first interact with Cdc37-kinase via previously published crystal structure contacts (Fig. 6C, state III). Whether assistance from Hsp70 and/or Hsp40, as with the glucocorticoid receptor, would be required is still unclear (*34*), but the inability to directly form the complex from components and Chk1 reconstitution experiments (*35*) is suggestive. During the cycle, Cdc37 would act as a quality-control checkpoint, where it would dissociate from the kinase only upon proper folding of the N lobe. The long coiled-coil would allow Cdc37-kinase to stay attached to Hsp90 during multiple ATP hydrolysis events. If the kinase would fail to dissociate after many hydrolysis events, the degradation machinery might then be recruited to the complex. Although Fig. 6C captures the essence of the available data, other models are possible.

Beyond revealing the kinase open state, our cryo-EM reconstruction allowed us to build the first atomic models for human cytosolic Hsp90 and the kinase-interacting N terminus of Cdc37. The ability to collect a large number of particles, coupled with the capabilities of single-electron–counting detectors and 3D classification software, allowed us to visualize multiple conformations, providing a qualitative assessment for the dynamic nature of the complex. Overall, our structure has enabled us to explain a number of often-contradictory biochemical observations and to provide both mechanistic and conceptual models of Hsp90-kinase interactions that can be tested in future experiments. Our structure also indicates the potential for single-particle cryo-EM to facilitate exploration of other dynamic, asymmetric complexes at near-atomic resolution.

### REFERENCES AND NOTES


1. S. S. Taylor, M. M. Keshwani, J. M. Steichen, A. P. Kornev, *Philos. Trans. R. Soc. Lond. B Biol. Sci.* **367**, 2517–2528 (2012).
2. J. Zhang, P. L. Yang, N. S. Gray, *Nat. Rev. Cancer* **9**, 28–39 (2009).
3. J. A. Endicott, M. E. Noble, L. N. Johnson, *Annu. Rev. Biochem.* **81**, 587–613 (2012).
4. J. Brugge, W. Yonemoto, D. Darrow, *Mol. Cell. Biol.* **3**, 9–19 (1983).
5. M. Taipale, D. F. Jarosz, S. Lindquist, *Nat. Rev. Mol. Cell Biol.* **11**, 515–528 (2010).
6. M. Taipale *et al.*, *Cell* **150**, 987–1001 (2012).
7. Y. Miyata, H. Nakamoto, L. Neckers, *Curr. Pharm. Des.* **19**, 347–365 (2013).
8. K. A. Krukenberg, T. O. Street, L. A. Lavery, D. A. Agard, *Q. Rev. Biophys.* **44**, 229–255 (2011).
9. M. P. Mayer, L. Le Breton, *Mol. Cell* **58**, 8–20 (2015).
10. D. R. Southworth, D. A. Agard, *Mol. Cell* **32**, 631–640 (2008).
11. S. Tsutsumi *et al.*, *Proc. Natl. Acad. Sci. U.S.A.* **109**, 2937–2942 (2012).
12. J. Shao, A. Irwin, S. D. Hartson, R. L. Matts, *Biochemistry* **42**, 12577–12588 (2003).
13. S. M. Roe *et al.*, *Cell* **116**, 87–98 (2004).
14. J. M. Eckl *et al.*, *J. Biol. Chem.* **288**, 16032–16042 (2013).
15. S. Polier *et al.*, *Nat. Chem. Biol.* **9**, 307–312 (2013).
16. C. K. Vaughan *et al.*, *Mol. Cell* **31**, 886–895 (2008).
17. M. Taipale *et al.*, *Nat. Biotechnol.* **31**, 630–637 (2013).
18. E. E. Boczek *et al.*, *Proc. Natl. Acad. Sci. U.S.A.* **112**, E3189–E3198 (2015).
19. C. K. Vaughan *et al.*, *Mol. Cell* **23**, 697–707 (2006).
20. Y. Cheng, *Cell* **161**, 450–457 (2015).
21. S. D. Hartson, V. Thulasiraman, W. Huang, L. Whitesell, R. L. Matts, *Biochemistry* **38**, 3837–3849 (1999).
22. Materials and methods are available as supplementary materials on *Science* Online.
23. M. M. Ali *et al.*, *Nature* **440**, 1013–1017 (2006).
24. T. Takaki *et al.*, *Proc. Natl. Acad. Sci. U.S.A.* **106**, 4171–4176 (2009).
25. O. Genest *et al.*, *Mol. Cell* **49**, 464–473 (2013).
26. L. A. Lavery *et al.*, *Mol. Cell* **53**, 330–343 (2014).
27. J. M. Eckl *et al.*, *J. Biol. Chem.* **290**, 30843–30854 (2015).
28. W. Liu, R. Landgraf, *Biochemistry* **54**, 1493–1504 (2015).
29. P. J. Day *et al.*, *Proc. Natl. Acad. Sci. U.S.A.* **106**, 4166–4170 (2009).
30. W. Xu *et al.*, *Nat. Struct. Mol. Biol.* **12**, 120–126 (2005).
31. J. Lachowiec, T. Lemus, E. Borenstein, C. Queitsch, *Mol. Biol. Evol.* **32**, 91–99 (2015).
32. O. Miyashita, J. N. Onuchic, P. G. Wolynes, *Proc. Natl. Acad. Sci. U.S.A.* **100**, 12570–12575 (2003).
33. Y. Shan, A. Arkhipov, E. T. Kim, A. C. Pan, D. E. Shaw, *Proc. Natl. Acad. Sci. U.S.A.* **110**, 7270–7275 (2013).
34. E. Kirschke, D. Goswami, D. Southworth, P. R. Griffin, D. A. Agard, *Cell* **157**, 1685–1697 (2014).
35. S. J. Arlander *et al.*, *J. Biol. Chem.* **281**, 2989–2998 (2006).
36. Single-letter abbreviations for the amino acid residues are as follows: A, Ala; C, Cys; D, Asp; E, Glu; F, Phe; G, Gly; H, His; I, Ile; K, Lys; L, Leu; M, Met; N, Asn; P, Pro; Q, Gln; R, Arg; S, Ser; T, Thr; V, Val; W, Trp; and Y, Tyr.


### ACKNOWLEDGMENTS

We thank members of NRAMM-Scripps for help with collecting data; Y. Fan for the yeast expression vector; N. Ohbayashi and M. Niino (RIKEN Center for Life Science Technologies) for help with Sf9 protein expression; N. F. Rebbe (University of North Carolina at Chapel Hill) and E. Laue (University of Cambridge) for the plasmids encoding human HSP90b and Cdc37, respectively; D.A.A.'s lab members for helpful discussions; and N. Jura for reading the manuscript. Support for this work was provided by Protein Structure Initiative–Biology grant U01 GM098254 (to D.A.A.), American Association for Cancer Research–Breast Cancer Research Foundation grant 218084 for Translational Breast Cancer Research (to D.A.A.), a gift from the Cabala family (to D.A.A.), an HHMI Helen Hay Whitney Foundation Fellowship (to Y.L.), an HHMI International Student Research Fellowship (to K.A.V.), and the HHMI (to D.A.A.). Some of the work presented here was conducted at NRAMM, which is supported by a grant from the NIH National Institute of General Medical Sciences (9 P41 GM103310). Some of the work used the Extreme Science and Engineering Discovery Environment (XSEDE), which is supported by NSF grant ACI-1053575.

### SUPPLEMENTARY MATERIALS

www.sciencemag.org/content/352/6293/1542/suppl/DC1
Materials and Methods
Figs. S1 to S13
Tables S1 and S2
References (*37*–*58*)
Movies S1 to S4

22 February 2016; accepted 13 May 2016
10.1126/science.aaf5023

QUANTUM SIMULATION

# Exploring the many-body localization transition in two dimensions

**Jae-yoon Choi,[1]*† Sebastian Hild,[1]* Johannes Zeiher,[1] Peter Schauß,[1]‡ Antonio Rubio-Abadal,[1] Tarik Yefsah,[1]§ Vedika Khemani,[2] David A. Huse,[2,3] Immanuel Bloch,[1,4] Christian Gross[1]**

**A fundamental assumption in statistical physics is that generic closed quantum many-body systems thermalize under their own dynamics. Recently, the emergence of many-body localized systems has questioned this concept and challenged our understanding of the connection between statistical physics and quantum mechanics. Here we report on the observation of a many-body localization transition between thermal and localized phases for bosons in a two-dimensional disordered optical lattice. With our single-site–resolved measurements, we track the relaxation dynamics of an initially prepared out-of-equilibrium density pattern and find strong evidence for a diverging length scale when approaching the localization transition. Our experiments represent a demonstration and in-depth characterization of many-body localization in a regime not accessible with state-of-the-art simulations on classical computers.**

In his seminal work on localization in quantum mechanical systems, Philip Anderson emphasized the implications of localization on the thermodynamics of closed quantum systems (*1*). Recently, perturbative arguments suggested the existence of nonthermalizing, many-body localized systems at low energy (*2*, *3*). Soon thereafter, these arguments were extended to all interaction strengths and energy densities for systems with a bounded spectrum (*4*, *5*). The implication—nothing less than a breakdown of equilibrium statistical mechanics for certain generic

**Atomic structure of Hsp90-Cdc37-Cdk4 reveals that Hsp90 traps and stabilizes an unfolded kinase**
Kliment A. Verba, Ray Yu-Ruei Wang, Akihiko Arakawa, Yanxin Liu, Mikako Shirouzu, Shigeyuki Yokoyama and David A. Agard (June 23, 2016)
*Science* **352** (6293), 1542-1547. [doi: 10.1126/science.aaf5023]

Editor's Summary

**Holding kinases at the ready**

About 60% of kinases only reach their active state in the presence of the molecular chaperone Hsp90 and its co-chaperone Cdc37. It is unclear how the chaperones facilitate kinase function or why only some kinases are chaperone-dependent. Verba *et al.* determined a 3.9 Å cryo–electron microscopy structure of Hsp90:Cdc37 in complex with the kinase Cdk4. Together, Hsp90 and Cdc37 trap the kinase in an open, partially unfolded state. Taking on this state probably has direct functional benefits.

*Science*, this issue p. 1542



*Science* (print ISSN 0036-8075; online ISSN 1095-9203) is published weekly, except the last week in December, by the American Association for the Advancement of Science, 1200 New York Avenue NW, Washington, DC 20005. 